ELSEVIER

Cement & Concrete Composites 24 (2002) 317–329

Cement & Concrete Composites

www.elsevier.com/locate/cemconcomp

Theoretical analysis of the effect of weak sodium sulfate solutions on the durability of concrete

J. Marchand [a,b,*], E. Samson [a,b], Y. Maltais [a,b], J.J. Beaudoin [c]

[a] CRIB – Department of Civil Engineering, Laval University, Ste-Foy, Que., Canada G1K 7P4

[b] SIMCO Technologies Inc. 1400, boul. du Parc Technologique, Quebec City, Que., Canada G1P 4R7

[c] Materials Laboratory, Institute for Research in Construction, National Research Council, Ottawa, Ont., Canada K1A 0R6

Abstract

A theoretical analysis of the detrimental influence of weak sodium sulfate solutions (Na_2SO_4) on the durability of concrete is presented. It was conducted using a numerical model that takes into account the coupled transport of ions and liquid and the chemical equilibrium of solid phases within the (partially) saturated system. Numerous simulations were performed to investigate the influence of various parameters such as water/cement (w/c) ratio (0.45, 0.65 and 0.75), type of cement (CSA Type 10 and Type 50), sulfate concentration (0–30 mmol/l of SO_4) and the gradient in relative humidity across the material. All input data related to the properties of concrete were obtained by testing well-cured laboratory mixtures. Numerical results indicate that exposure to weak sulfate solutions can result in a significant reorganization of the microstructure of concrete. The penetration of sulfate ions into the material is not only at the origin of the precipitation of sulfate-bearing phases (such as ettringite and eventually gypsum) but also results in calcium hydroxide dissolution and C–S–H decalcification. Data also clearly emphasize the fact that w/c ratio remains the key parameter that controls the durability of concrete to sulfate attack.

Keywords: Sulfate solution; Concrete; Theoretical analysis

1. Introduction

Concrete subjected to sulfate attack can undergo a progressive and profound reorganization of its internal microstructure [1–6]. These alterations have direct consequences on the engineering properties of the material. For instance, concrete undergoing sulfate attack is often found to suffer from swelling, spalling and cracking [1,6–8]. There is also overwhelming evidence to show that the degradation also contributes to a significant reduction of the mechanical properties of concrete [6,9–12]. Many structures affected by sulfate degradation often need to be repaired or, in the most severe cases, partially reconstructed.

Given the deleterious effects of sulfate attack, building codes have traditionally specified precautionary measures to protect concrete against this type of degradation. Typical measures contained in North American building codes [13–16] are summarized in Table 1. As can be seen, the choice of cement (ASTM Type I, Type II, Type V or the equivalent) and the selection of water/cement (w/c) ratio vary according to the severity of the exposure conditions.

It should be emphasized that recommendations concerning concrete exposed to negligible sulfate concentrations (i.e. soils containing less than 0.10% of water soluble sulfate or solutions for which the SO_4 concentration is less than 150 ppm) are relatively vague. Although building codes usually emphasize the importance of limiting the permeability of concrete to prevent the penetration of moisture and ions, [1] none of them contains any specific limit concerning the maximum w/c ratio that should be selected for the production of concrete elements to be exposed to negligible levels of sulfate (see Table 1). This is unfortunate since, as emphasized by many authors, potentially destructive conditions may exist even though analyses indicate the ground water or

* Corresponding author. Tel.: +418-656-2079; fax: +418-656-3355.
E-mail address: jacques.marchand@gci.ulaval.ca (J. Marchand).

[1] For instance, the Canadian Standard [16] limits the w/c ratio of concrete exposed to salts without any freezing and thawing to 0.55. Similarly, in its Concrete Craftsman Series, the American Concrete Institute (ACI) [17] recommends a limit w/c ratio of 0.7 for concrete to be used for the construction of slabs on grade.

0958-9465/02/$ - see front matter
PII: S0958-9465(01)00083-X

Table 1
Recommendations for protecting concrete exposed to sulfate contaminated environments (from [13–16])

Exposure	Water soluble sulfate (SO_4) in soil, %	Sulfate (SO_4) in water, ppm	Cement	w/c ratio, maximum
Mild	0.00–0.10	0–150	–	–
Moderate	0.10–0.20	150–1500	Type II, IP (MS), IS (MS)	0.50
Severe	0.20–2.00	1500–10 000	Type V	0.45
Very severe	Over 2.00	Over 10 000	Type V + pozzolan or slag	0.45

soil to have a low sulfate content [18–20]. According to DePuy [20], this is apparently often the case when concrete is exposed to wetting and drying cycles.

The present study was conducted to provide additional information on the potentially deleterious effects of weak sulfate solutions on the behavior of concrete. A numerical model, called STADIUM, [2] was used to investigate the mechanisms of degradation. This model takes into account the coupled transport of ions and liquid and the chemical equilibrium of solid phases within the (partially) saturated system. Previous studies have indicated that numerical results yielded by the model for hydrated cement systems subjected to sulfate attack and calcium leaching compare favorably to those measured experimentally [21–23].

2. Description of the numerical model

2.1. Description of the various transport processes

STADIUM has been developed to predict the transport of ions in unsaturated porous media. As will be discussed in the following subsection, the model also accounts for the effect of dissolution/precipitation reactions on the transport mechanisms.

The description of the various transport mechanisms relies on the homogenization technique. This approach first requires writing all the basic equations at the pore scale. These equations are then averaged over a representative elementary volume (REV) in order to describe the transport mechanisms at the macroscopic scale. More information on the transport equations at the pore scale and the averaging technique can be found in [24–26].

In the model, ions are considered to be either free to move in the liquid phase or bound to the solid phase. The transport of ions in the liquid phase at pore scale is described by the extended Nernst–Planck equation [27] to which an advection term is added [26]. After integrating this equation over the REV, the transport equation becomes

$$\frac{\partial(\theta_s C_{is})}{\partial t}+\frac{\partial(\theta C_i)}{\partial t}-\frac{\partial}{\partial x}\left(\theta D_i\frac{\partial C_i}{\partial x}+\theta\frac{D_i z_i F}{RT}C_i\frac{\partial \Psi}{\partial x}+\theta D_i C_i\frac{\partial \ln\gamma_i}{\partial x}-C_i V_x\right)=0. \quad (1)$$

In Eq. (1), θ_s is the solid content of the material, C_i is the concentration of the species i in the aqueous phase, C_{is} is the concentration of the solid phase, θ is the volumetric water content, D_i is the diffusion coefficient, z_i is the valence number of the species, F is the Faraday constant, R is the ideal gas constant, T is the temperature of the liquid, Ψ is the electrical potential, γ_i is the chemical activity coefficient and V_x is the velocity of the fluid.

Eq. (1) has to be written for each ionic species present in the system. Previous experience [21–23] has shown that the behavior of hydrated cement materials (in chloride and magnesium free environments) can be reliably described by considering six different ionic species: OH^-, Na^+, K^+, SO_4^{2-}, Ca^{2+} and $Al(OH)_4^-$.

To calculate the chemical activity coefficients, several approaches are available. However, classical models such as those proposed by Debye–Hückel or Davies are unable to reliably describe the thermodynamic behavior of highly concentrated electrolytes such as the hydrated cement paste pore solution [28]. A modification of the Davies equation was found to yield good results [29]

$$\ln\gamma_i=-\frac{Az_i^2\sqrt{I}}{1+a_iB\sqrt{I}}+\frac{(0.2-4.17\times10^{-5}I)Az_i^2I}{\sqrt{1000}}, \quad (2)$$

where I is the ionic strength of the solution

$$I=\frac{1}{2}\sum_{i=1}^{N}z_i^2c_i \quad (3)$$

and A and B are the temperature-dependent parameters. The parameter a_i in Eq. (2) depends on the ionic species. Its value (in meters) is 3×10^{-10} for OH^-, 3×10^{-10} for Na^+, 3.3×10^{-10} for K^+, 1×10^{-10} for SO_4^{2-}, 2×10^{-10} for Cl^- and 1×10^{-13} for Ca^{2+} [29].

A last relation is required to complete the system of equations and calculate the electrical potential Ψ appearing in Eq. (1). This can be done using the Poisson equation, which relates the electrical potential to the concentration of each ionic species [30,31]. The equation is given here in its averaged form

[2] STADIUM stands for Software for Transport And Degradation In (Un)saturated Materials.

Table 2
Equilibrium constants for solid phases in hydrated cement systems

Name	Chemical composition	Expression for equilibrium	Value of equilibrium constant ($-\log K_{sp}$)
Portlandite	$Ca(OH)_2$	$K_{sp} = \{Ca\}\{OH\}^2$	5.2
C–S–H	$1.65CaO \cdot SiO_2 \cdot (2.45)H_2O$[a]	$K_{sp} = \{Ca\}\{OH\}^{2}$[b]	5.6[b]
Ettringite	$3CaO \cdot Al_2O_3 \cdot 3CaSO_4 \cdot 32H_2O$	$K_{sp} = \{Ca\}^6\{OH\}^4\{SO_4\}^3\{Al(OH)_4\}^2$	44.0
Hydrogarnet	$3CaO \cdot Al_2O_3 \cdot 6H_2O$	$K_{sp} = \{Ca\}^3\{OH\}^4\{Al(OH)_4\}^2$	23.0
Gypsum	$CaSO_4 \cdot 2H_2O$	$K_{sp} = \{Ca\}\{SO_4\}$	4.6

{...} indicates chemical activity.
[a] C–S–H is assumed to have a C/S ratio of 1.65.
[b] The C–S–H decalcification is modeled as the portlandite dissolution with a lower solubility.

$$\frac{\partial}{\partial x}\left(\theta\tau\frac{\partial \Psi}{\partial x}\right) + \theta\frac{F}{\epsilon}\sum_{i=1}^{N} z_i C_i = 0, \tag{4}$$

where N is the total number of ionic species, ϵ is the dielectric permitivity of the medium, in this case water, and τ is the tortuosity of the porous network. The physical meaning of the tortuosity coefficient is discussed in [25,26].

The velocity of the fluid, appearing in Eq. (1) as V_x, can be described by a diffusion equation when the driving force for the movement of water is linked to the capillary forces arising in the porous solid during drying/wetting cycles [32]

$$V_x = -D_w\frac{\partial\theta}{\partial x}, \tag{5}$$

where D_w is the non-linear water diffusion coefficient. This parameter varies according to the water content of the material [32].

To complete the model, the mass conservation on the liquid phase must be taken into account [32]

$$\frac{\partial\theta}{\partial t} - \frac{\partial}{\partial x}\left(D_w\frac{\partial\theta}{\partial x}\right) = 0. \tag{6}$$

As can be seen, moisture transport is described in terms of a variation of the (liquid) water content of the material. It should be emphasized that the choice of using the material water content as the state variable for the description of this problem has an important implication on the treatment of the boundary conditions. Since the latter are usually expressed in terms of relative humidity, a conversion has to be made. This can be done using an adsorption/desorption isotherm [32].

The system of non-linear equations has to be solved numerically. Information on the numerical resolution of the problem using the finite element method can be found in [30,31].

2.2. Chemical equilibrium step

The first term on the left-hand side of Eq. (1) (in which C_{is} appears) accounts for the ionic exchange between the solution and the solid. It can be used to model the influence of precipitation/dissolution reactions on the transport process. The chemical equilibrium of the various solid phases present in the material is verified at each node of the finite element mesh by considering the concentrations of all ionic species at this location. If the equilibrium condition is not respected, the concentrations and the solid phase content are corrected accordingly.

For instance, the equilibrium constant of calcium hydroxide (or portlandite) is given by

$$K_{sp} = \{Ca\}\{OH\}^2, \tag{7}$$

where the curly brackets $\{\cdots\}$ indicate chemical activity. As previously mentioned, Eq. (7) must be verified at each node within the system. If, due to the transport process, the solution is locally supersaturated or undersaturated, the concentration of ions is corrected to restore the chemical equilibrium. This procedure is applied at each node to each solid phase present in the system.

Previous experience [21,23] has shown that the behavior of hydrated cement systems exposed to relatively weak sodium sulfate (Na_2SO_4) solutions could be well described by considering five different solid phases, namely: portlandite, C–S–H, ettringite, hydrogarnet, and gypsum. These phases are listed in Table 2, along with their equilibrium constant [33].

Obviously, the treatment of an ill-crystallized phase such as the C–S–H presents some difficulties. As can be seen in Table 2, an apparent equilibrium constant is attributed to the C–S–H. The value of this constant was established on the basis of previously published reports on the thermodynamic stability of hydrated cement systems [34,35]. The *dissolution* of C–S–H (the so-called decalcification process) is assumed to proceed by the release of calcium and hydroxide ions (in a proportion of one Ca^{2+} to two OH^- in order to maintain the electroneutrality of the solution) leaving behind a silica gel. This approach is in good agreement with the observation of Faucon [36] who could analyze the composition of decalcified C–S–H using nuclear magnetic resonance (NMR) spectroscopy and Mössbauer spectroscopy (such as NMR).

Table 3
Characteristics of the concrete mixtures

	$w/c = 0.45$	$w/c = 0.65$	$w/c = 0.75$
Cement (kg/m^3)	380.0	280.0	250.0
Water (kg/m^3)	171.0	182.0	187.5
Sand (kg/m^3)	719.0	833.0	931.0
Coarse aggregate (kg/m^3)	1127.0	1065.0	972.7
Volumetric paste content (%)	29.2	27.1	26.7

Chemical reactions can also modify the transport properties of the material by affecting its pore structure. For instance, the precipitation of gypsum may contribute to locally reduce the porosity of the material, thus decreasing the section across which ions are able to diffuse. This may have an effect on the diffusion coefficient of the material. This effect is taken into account using the equation proposed by Garboczi and Bentz [37]

$$\frac{D_i}{D_i^{\mu}} = 0.001 + 0.07\phi_{\text{cap}}^2 + 1.8 \times H(\phi_{\text{cap}} - 0.18)(\phi_{\text{cap}} - 0.18)^2, \quad (8)$$

where ϕ_{cap} is the capillary porosity of the paste, D_i^{μ} is the diffusion coefficient of the ionic species i in free solution (as opposed to its diffusion coefficient in the porous solid) and H is the Heaviside function such that $H(x) = 1$ for $x > 0$ and $H(x) = 0$ for $x \leqslant 0$. The initial capillary porosity of the material can be calculated using the following relationship [38]:

$$\phi_{\text{cap}}^{\text{init}} = \frac{(w/c) - 0.36\alpha}{(w/c) + 0.32}, \quad (9)$$

where w/c is the water/cement ratio of the paste and α is the degree of hydration cement ($0 \leqslant \alpha \leqslant 1$). The influence of chemical reactions on the capillary porosity of the material can be calculated as follows:

$$\phi_{\text{cap}} = \phi_{\text{cap}}^{\text{init}} + \sum_{s=1}^{M} (V_{\text{s}}^{\text{init}} - V_{\text{s}}), \quad (10)$$

where V_{s} is the volume of a given solid phase, per unit volume of cement paste, and M is the total number of solid phases. According to this approach, the correction factor G that multiplies the diffusion coefficients D_i of each ionic species is given by

$$G = \frac{\left.\frac{D_i}{D_i^{\mu}}\right|_{\text{Modified paste}}}{\left.\frac{D_i}{D_i^{\mu}}\right|_{\text{Initial paste}}}. \quad (11)$$

The application of Eqs. (10) and (11) to description of the influence of the C–S–H decalcification process on the diffusion properties of hydrated cement systems presents some obvious problems. Within the framework of this investigation, the value of the correction factor G has been arbitrarily fixed at 10 for fully decalcified systems. Sensitivity analyses have indicated that the value of this factor (for the decalcified C–S–H) has little influence on the kinetics of degradation [39].

3. Characteristics of the materials

In order to obtain the input data required to run the model, six different concrete mixtures were cast and tested. Test variables included type of cement (CSA Type 10 and CSA Type 50) and w/c ratio (0.45, 0.65 and 0.75). The characteristics of the six concrete mixtures are given in Table 3 and the chemical and mineralogical compositions of the two cements are summarized in Table 4.

All mixtures were prepared with a natural siliceous sand and a crushed granitic stone. The maximum size of the coarse aggregates used to prepare the concrete mixture was 14 mm.

All mixtures were prepared in a counter-current pan mixer (capacity = 0.1 m^3). The aggregates (coarse and fine) and the cement were first introduced in the mixer, and mixed for 1 min to homogenize the materials. Water was then added to the dry materials over a period of 30 s. Concrete was initially mixed for 3 min. After a pause of 3 min, concrete was mixed for another 2 min. The

Table 4
Chemical and mineralogical analyses of the cements

Oxides	Type 10	Type 50
SiO_2	20.4	22.5
Al_2O_3	4.3	3.0
Fe_2O_3	3.0	3.7
CaO	62.1	63.5
MgO	2.8	3.2
SO_3	3.2	2.0
Na_2O	n/d	0.2
K_2O	n/d	0.4
Na_2O eq.	0.8	0.4
Free CaO	1.0	0.8
Loss on ignition	2.0	1.1
Insoluble residue	0.6	0.2
Bogue analysis		
C_3S	55.4	56.3
C_2S	16.7	22.0
C_3A	6.3	1.7
C_4AF	9.1	11.3

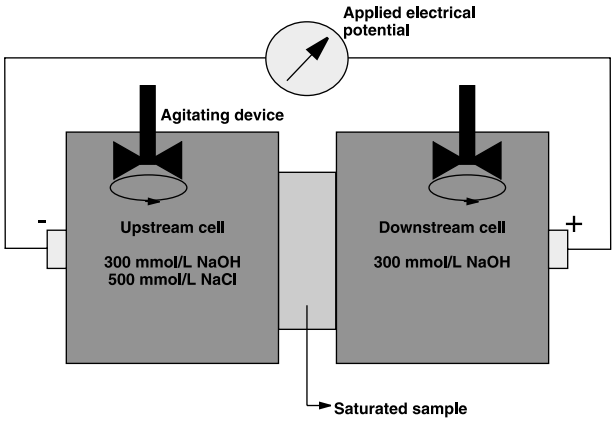

Fig. 1. Experimental set-up for the migration test.

concrete was then periodically mixed for 30 s every 5 min over a 20-min period in order to simulate continuous mixing.

The fresh concrete mixtures were cast in plastic molds (diameter = 100 mm and height = 200 mm). The molds were filled in three layers in accordance with the requirements of CSA A23.2–3C (the Canadian version of ASTM C192/C 192M-95). Samples were demolded approximately 24 h after casting, and sealed in an aluminum foil for 91 days in order to avoid any exchange of moisture with the surrounding environment.

At the end of the curing period, 25-mm thick disks were cut and tested for chloride migration. Migration tests were used to determine the diffusion coefficients of the ionic species in the various mixtures. Prior to testing, all samples were first immersed in a 300 mmol/l NaOH solution and vacuum saturated for about 48 h. After this saturation period, samples were mounted on a migration cell consisting of two compartments (individual capacity of 3 l) as shown in Fig. 1. The upstream compartment was filled with a solution of 300 mmol/l NaOH and 500 mmol/l NaCl, while a 300 mmol/l NaOH solution was placed in the downstream compartment. The high pH of the test solutions contributes to minimize the risk of microstructural alterations during the experiment. An electrical potential of about 12 V was then applied on the migration set-up in order to accelerate the transport of chlorides through the sample. A constant temperature of 23 °C was maintained during the entire duration of the test.

The current circulating through the system was regularly measured during the test, which lasted for about five days. A special version of STADIUM, called STADIUM-ACC, was used to analyze the migration test data and calculate the diffusion coefficients. More information on the analysis can be found elsewhere (see [39]). Results are summarized in Tables 5 and 6.

The pore solution of each mixture was also extracted and analyzed according to the procedure described by Longuet et al. [40] and Diamond [41]. Samples were

Table 5
Materials properties used to perform the numerical simulations – CSA Type 10 mixtures

Properties	Type 10 cement		
	$w/c = 0.45$	$w/c = 0.65$	$w/c = 0.75$
Diffusion coefficients (m^2/s)			
OH^-	10.8e – 11	19.5e – 11	29.4e – 11
Na^+	2.7e – 11	4.9e – 11	7.4e – 11
K^+	4.0e – 11	7.2e – 11	10.9e – 11
SO_4^{2-}	2.2e – 11	3.9e – 11	5.9e – 11
Ca^{2+}	1.6e – 11	2.9e – 11	4.4e – 11
$Al(OH)_4^-$	1.1e – 11	2.0e – 11	3.0e – 11
Water diffusivity (m^2/s)	$3.42 \times 10^{-11} e^{400}$	$3.34 \times 10^{-12} e^{750}$	$3.33 \times 10^{-12} e^{770}$
Initial pore solution (*mmol/l*)			
OH^-	427.97	269.42	268.94
Na^+	185.00	133.50	133.10
K^+	266.50	140.10	137.80
SO_4^{2-}	12.97	3.77	2.95
Ca^{2+}	1.25	1.70	2.00
$Al(OH)_4^-$	0.08	0.05	0.04
Porosity (%)	12.6	13.0	14.7
Tortuosity	0.020	0.037	0.056
Initial solid phase (*g/kg*)			
Portlandite	48.5	36.3	32.6
C–S–H	92.2	69.0	62.1
Ettringite	26.5	19.8	17.9
Hydrogarnet	11.7	8.7	7.9

Table 6
Materials properties used to perform the numerical simulations – CSA Type 50 mixtures

Properties	Type 50 cement		
	$w/c = 0.45$	$w/c = 0.65$	$w/c = 0.75$
Diffusion coefficients (m^2/s)			
OH^-	17.0e – 11	25.8e – 11	33.5e – 11
Na^+	4.3e – 11	6.5e – 11	8.5e – 11
K^+	6.3e – 11	9.6e – 11	12.4e – 11
SO_4^{2-}	3.4e – 11	5.2e – 11	6.8e – 11
Ca^{2+}	2.6e – 11	3.9e – 11	5.0e – 11
$Al(OH)_4^-$	1.7e – 11	2.7e – 11	3.4e – 11
Water diffusivity (m^2/s)	$3.42 \times 10^{-11} e^{400}$	$3.34 \times 10^{-12} e^{750}$	$3.33 \times 10^{-12} e^{770}$
Initial pore solution (*mmol/l*)			
OH^-	224.47	183.42	98.96
Na^+	107.10	71.40	55.50
K^+	116.50	108.90	34.30
SO_4^{2-}	1.88	1.17	0.30
Ca^{2+}	2.33	2.74	4.89
$Al(OH)_4^-$	0.03	0.03	0.02
Porosity (%)	12.2	13.6	15.3
Tortuosity	0.032	0.049	0.064
Initial solid phase (*g/kg*)			
Portlandite	51.0	38.1	34.3
C–S–H	101.7	76.1	68.5
Ettringite	16.6	12.4	11.2
Hydrogarnet	5.7	4.3	3.8

placed in an extraction cell and crushed at a pressure of approximately 300 MPa. Typically, 2–5 ml of pore solution were extracted. The solution was delivered through a drain ring and channel, and recovered with a syringe in order to limit exposure to the atmosphere. Chemical analyses of the pore solution were carried out shortly after the extraction test. The composition of the solution was then adjusted in order to respect the electroneutrality condition. Slight deviations from electroneutrality can arise due to the experimental error associated with the extraction procedure. The adjusted pore solution data are given in Tables 5 and 6.

Another series of samples were used for porosity measurements, which were carried out according to the requirements of ASTM C 642. Results are also presented in Tables 5 and 6.

The water diffusion properties of the six mixtures were estimated on the basis of nuclear magnetic resonance imaging (NMRI) measurements performed on companion mortar mixtures [42]. The diffusion coefficients of water used in the simulations are summarized in Tables 5 and 6.

In order to run the model, one has to know the initial amount of each solid phase in the material. The initial amounts of calcium hydroxide and C–S–H were calculated assuming a complete hydration ($\alpha = 1$) of the C_2S and C_3S contained in the cement (see Table 2), and using the following equations:

$$2(3CaO \cdot SiO_2) + 6H_2O \rightarrow 3CaO \cdot 2SiO_2 \cdot 3H_2O + 3(CaO \cdot H_2O) \quad (12)$$

$$2(2CaO \cdot SiO_2) + 4H_2O \rightarrow 3CaO \cdot 2SiO_2 \cdot 3H_2O + CaO \cdot H_2O \quad (13)$$

The initial amount of ettringite ($3CaO \cdot Al_2O_3 \cdot 3CaSO_4 \cdot 32H_2O$) was calculated by considering that all the gypsum added to the unhydrated cement had reacted with the C_3A. The remaining C_3A, and 50% of the alumina contained in the C_4AF, was assumed to have reacted to form hydrogarnet ($3CaO \cdot Al_2O_3 \cdot 6H_2O$). The calculated quantities are given in Tables 5 and 6.

4. Description of the numerical simulations

4.1. General information

The typical case of a concrete slab resting on a sulfate contaminated soil was considered in all the numerical simulations. In all cases, the thickness of the slab was fixed at 15 cm and the bottom part of the slab was considered to be directly in contact with the soil (containing Na^+ and SO_4^{2-} ions). Furthermore, it was assumed that the top surface of the slab was free of any barrier and directly in contact with the external environment.

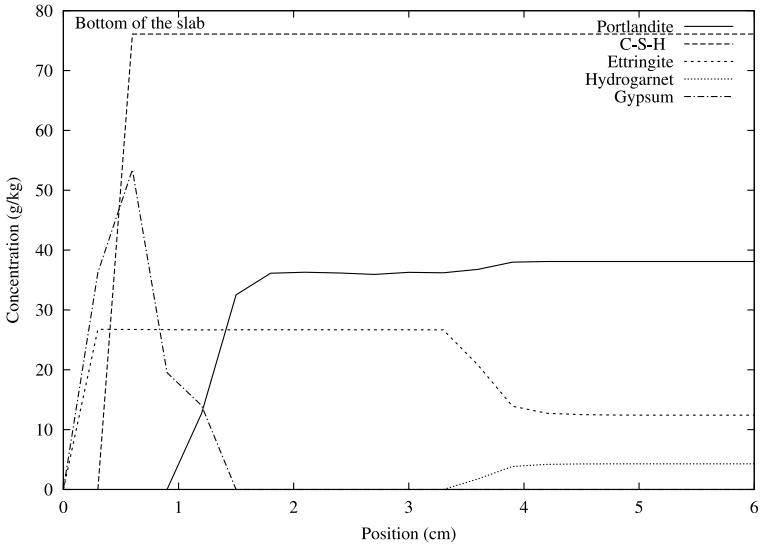

Fig. 2. Distribution of the solid phases after 20 years for the 0.65 w/c ratio concrete made with the CSA Type 50 cement and exposed to 10 mmol/l of sulfates – saturated conditions.

All simulations were performed assuming that the concrete slab was kept in isothermal conditions at 25 °C. Furthermore, the effects of carbonation were not taken into account in the numerical simulations.

4.2. Boundary conditions

In all the numerical simulations, the boundary conditions were kept constant during the entire service-life of the concrete. Two types of exposure conditions were taken into consideration. In the first case, the bottom surface of the (saturated) concrete slab was assumed to be in direct contact with a fully saturated soil (relative humidity equal to 100%). The air above the slab was also maintained at 100% relative humidity. In this initial case, ions were essentially transported by diffusion, the flux of water by capillary suction being nil.

In the second series of simulations, the bottom portion of the slab was assumed to be in contact with a partially saturated soil (relative humidity equal to 90%) and the air above the slab was kept at 75% relative humidity. In this second case, ions were transported by diffusion and advection (capillary suction) in the partially saturated concrete.

In all cases, the soil in contact with the concrete slab was considered to be contaminated with a sodium sulfate solution. Simulations were run for five different concentrations in SO_4 ranging from 0 to 30 mmol/l (i.e. from 0 to 60 mmol/l of Na^+). The concentration of all other ions (except Na^+ and SO_4^{2-}) was assumed to be equal to zero. In all simulations, the ionic flux near the upper part of the slab was considered to be zero.

4.3. Initial conditions

In all the simulations, the concrete was considered to be initially undamaged. The initial value of the potential Ψ was fixed at zero everywhere in the material. The potential was also maintained at zero on the lower part of the slab during the simulations, in order to establish a reference point. The initial composition of the pore solution and the porosity of all mixtures are given in Tables 5 and 6.

5. Results of the numerical simulations

Numerical simulations indicate that the exposure of concrete to weak sodium sulfate solutions can result in an important reorganization of its internal microstructure. A typical example is shown in Fig. 2 where the distribution in calcium hydroxide (portlandite), C–S–H, ettringite, hydrogarnet and gypsum is given for a 0.65 w/c ratio concrete made of a CSA Type 50 cement and that had been exposed in saturated conditions to 10 mmol of sulfate for 20 years. As indicated in the figure, the left-hand side of the graph corresponds to the surface of the slab in direct contact with the soil (bottom portion).

Fig. 2 indicates that the reorganization of the internal microstructure of concrete is characterized by the presence of degradation *fronts* that penetrate from the external (bottom) surface of the slab towards the center of the slab. These results are also in good agreement with most investigations that the microstructure of concrete subjected to external sulfate attack is usually

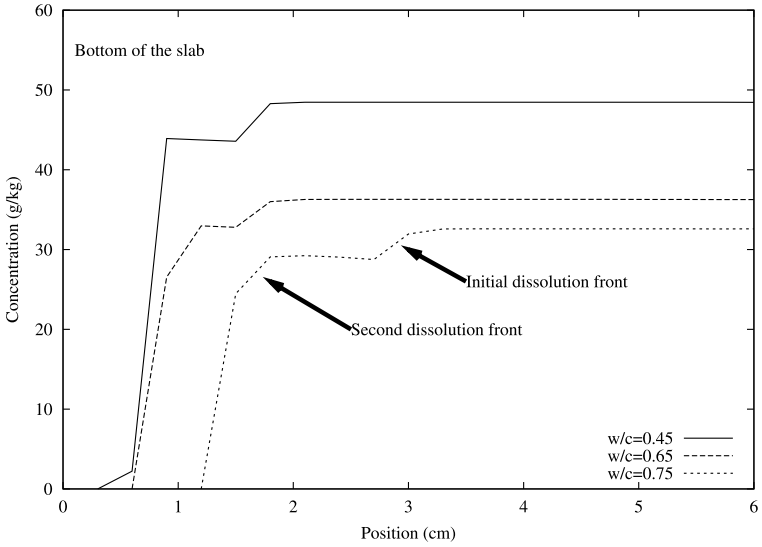

Fig. 3. Calcium hydroxide profiles after 20 years for the concrete mixtures made with the CSA Type 10 cement and exposed to 10 mmol/l of sulfates – saturated conditions.

characterized by a succession of layers (or zones) starting from the outer surface of the material [2–5,43].

As shown in Fig. 2, the exposure to the sodium sulfate solution has resulted in the formation of additional ettringite. It is important to note that even if the external concentration in SO_4^{2-} was relatively weak, the model also predicts the formation of gypsum. This result is in good agreement with field observations [1,18,19,44].

The precipitation of new sulfate-bearing phases is also accompanied by the dissolution of calcium hydroxide and hydrogarnet and by the decalcification of C–S–H. These phenomena are usually observed for laboratory and field concrete mixtures exposed to sulfate solutions [1–5]. During the degradation process, hydrogarnet is mainly consumed by a series of dissolution/precipitation reactions leading to the formation of ettringite. As can be seen in the figure, the initial amount of hydrogarnet limits the quantity of ettringite that can be formed during the degradation process. Once all the hydrogarnet is dissolved, the source of aluminum has vanished, which impedes the further precipitation of ettringite.

The dissolution of portlandite and the decalcification of C–S–H mainly occur due to the leaching of Ca^{2+} and

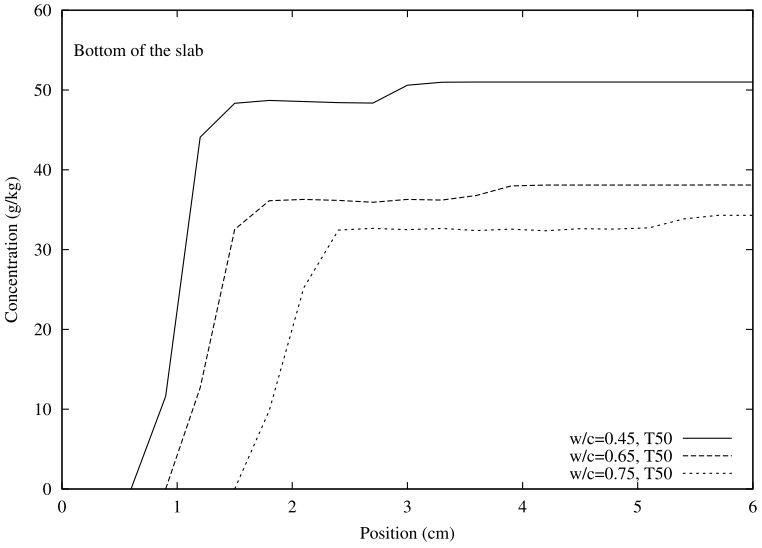

Fig. 4. Calcium hydroxide profiles after 20 years for the concrete mixtures made with the CSA Type 50 cement and exposed to 10 mmol/l of sulfates – saturated conditions.

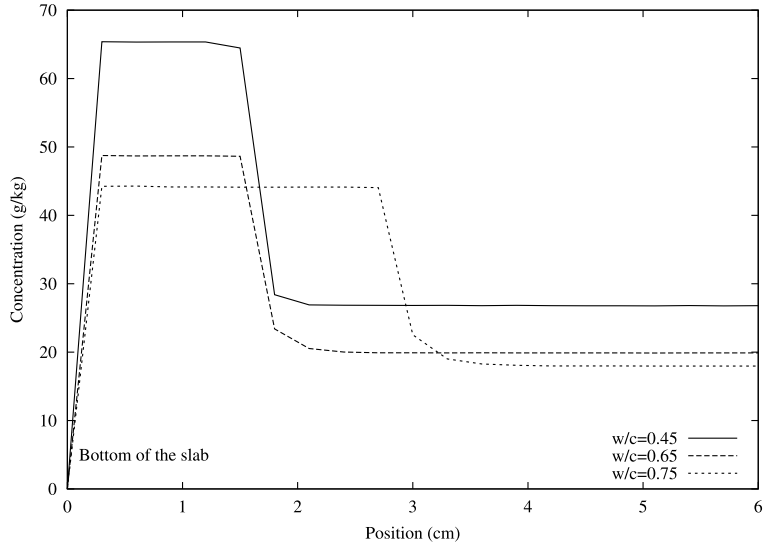

Fig. 5. Ettringite profiles after 20 years for the concrete mixtures made with the CSA Type 10 cement and exposed to 10 mmol/l of sulfates – saturated conditions.

OH^- ions that are diffusing out of the system (see the second dissolution front in Fig. 3). To supply the amount of calcium for the formation of ettringite, a slight portion of portlandite is also consumed ahead of the main dissolution front (see the first dissolution front in Fig. 3).

As previously mentioned, there is overwhelming evidence to show that the microstructural alterations resulting from sulfate attack contribute to significantly reduce the mechanical properties of concrete [6,9–12]. SEM observations tend to indicate that this reduction is, at least in part, associated with the local development of microcracks induced by the formation of new sulfate-bearing phases. Over the past decades, numerous studies have also clearly emphasized the detrimental influence of portlandite dissolution on the mechanical properties of hydrated cement systems [10,45–47]. It should be noted that the decalcification of the C–S–H is, most probably, the most severe degradation that can happen to a concrete mixture. As previously mentioned, the gradual leaching of calcium from the C–S–H leaves a residual silica gel. This gel is extremely porous and permeable and has no binding capacity.

Numerical simulations also indicate that the kinetics of degradation is mainly controlled by the diffusion coefficient of the material (see Figs. 3–6). These results

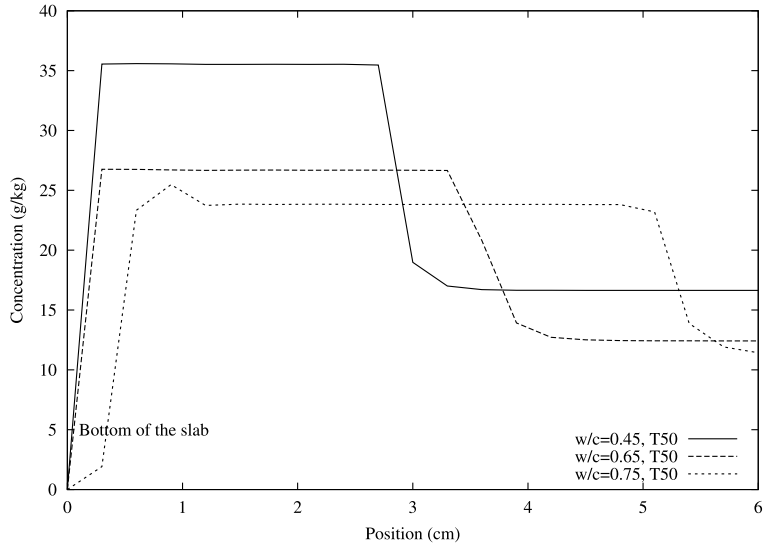

Fig. 6. Ettringite profiles after 20 years for the concrete mixtures made with the CSA Type 50 cement and exposed to 10 mmol/l of sulfates – saturated conditions.

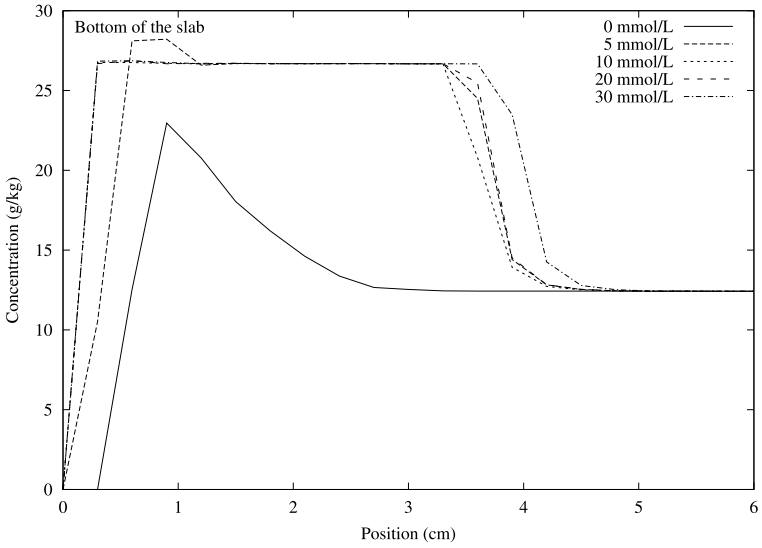

Fig. 7. Ettringite profiles after 20 years for the 0.65 w/c ratio concrete made with the CSA Type 50 cement and exposed to different sulfate concentrations – saturated conditions.

clearly emphasize the importance of limiting the w/c ratio below a certain critical value. As can be seen, while the two mixtures prepared at a w/c ratio of 0.45 do not exhibit any significant degradation after 20 years of exposure, the more porous mixtures are markedly affected by the exposure to the sulfate solution. It is noteworthy that the reduction of the w/c ratio does not modify the mechanisms of deterioration but simply reduces the kinetics of attack. The profiles for the 0.45 type 10, and 0.65 type 10 concrete mixtures shown in the four figures are very similar, despite very different diffusion coefficients.

It is emphasized that the use of a sulfate-resisting cement is not a sufficient measure to protect concrete against degradation, even when the structure is exposed to weak concentrations of SO_4^{2-}. These results are in good agreement with the observations of many authors [1,19,20,44]. In the present study, the slightly detrimental influence of the sulfate-resisting cement on the kinetics of degradation might be attributed to its effect on the diffusion coefficient of concrete. As can be seen in Table 3, the use of the CSA Type 50 cement has contributed to increase the diffusion coefficient

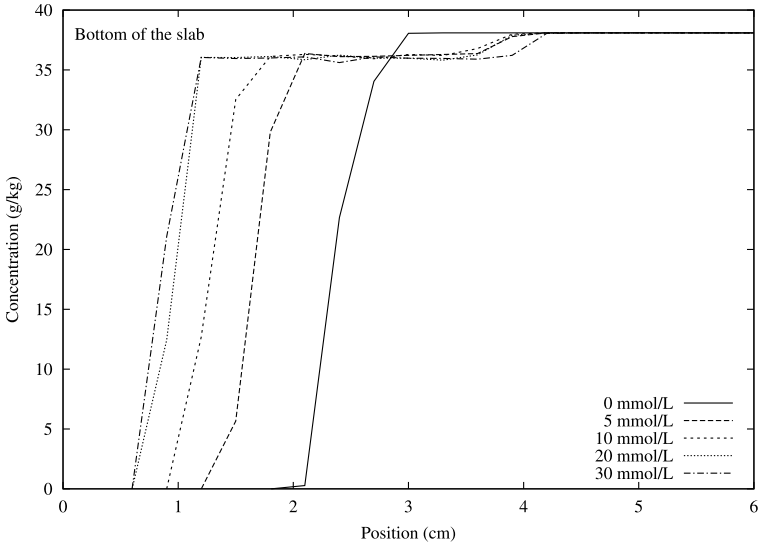

Fig. 8. Calcium hydroxide profiles after 20 years for the 0.65 w/c ratio concrete made with the CSA Type 50 cement and exposed to different sulfate concentrations – saturated conditions.

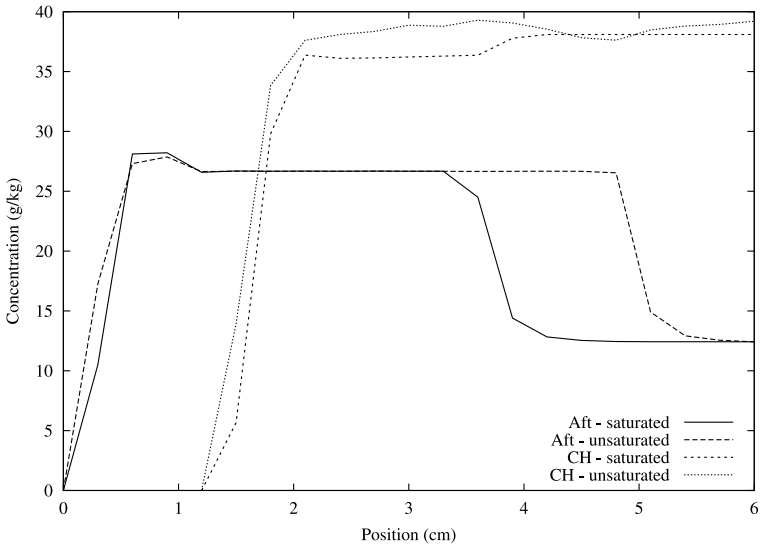

Fig. 9. Ettringite profiles after 20 years for the 0.65 w/c ratio concrete made with the CSA Type 50 cement and exposed to 5 mmol/l of sulfate – unsaturated conditions.

of all concrete mixtures whatever the w/c ratio. This phenomenon is discussed in more detail in [48].

As shown in Fig. 7, an increase of the SO_4^{2-} concentration of the external solution (from 5 to 30 mmol/l) contributes only to a slight acceleration of the kinetics of penetration of the ettringite front. It is also interesting to note that the model predicts the formation of a weak peak of ettringite for the 0 mmol/l case, i.e. the case without any external sulfate. Its presence is due to the dissolution of ettringite near the bottom of the slab. As a result of diffusion and the electrical coupling, the $Al(OH)_4^-$ ions move deeper into the material after this dissolution and precipitate to form this peak.

The external SO_4^{2-} concentration has a more significant effect on the kinetics of portlandite dissolution (see Fig. 8). An increase in the SO_4^{2-} concentration tends to slightly accelerate the initial dissolution of calcium hydroxide. Subsequently, the formation of ettringite contributes to reduce the progression of the main portlandite dissolution front. This phenomenon is linked to the fact that the precipitation of ettringite results in a local reduction of porosity of the material. However, these results should be considered with caution. The influence of microcracks (induced by the formation of ettringite and gypsum) is not taken into account by the model.

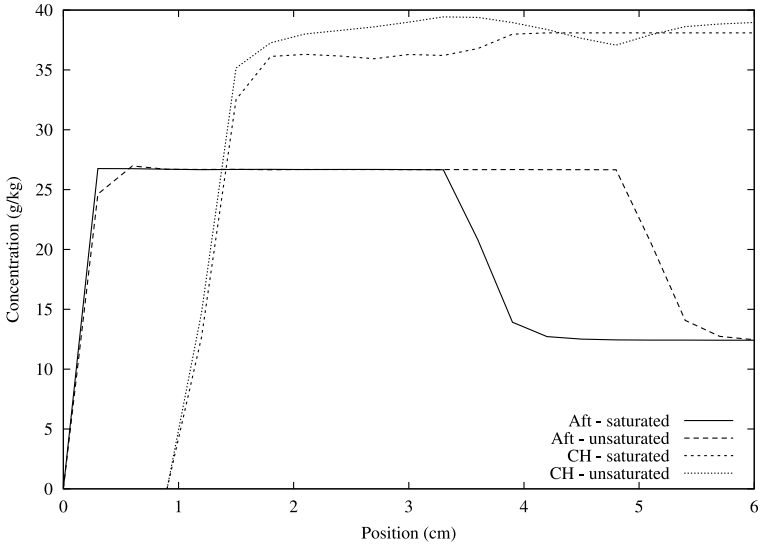

Fig. 10. Calcium hydroxide profiles after 20 years for the 0.65 w/c ratio concrete made with the CSA Type 50 cement and exposed to 5 mmol/l of sulfate – unsaturated conditions.

Finally, numerical results clearly indicate that the detrimental influence of weak sodium sulfate solutions is not predominantly due the suction of SO_4^{2-} ions by capillary forces. As can be seen in Figs. 9 and 10, the transport of water by capillary suction does not seem to have any significant effect on the behavior of concrete. These results are in good agreement with SEM observations and microprobe analyses recently made on a series of laboratory mixtures [48]. It should however be borne in mind that wetting and drying cycles may result in cracking and spalling especially for porous concrete mixtures [7,8].

6. Concluding remarks

Numerical simulations indicate that the exposure to weak sodium sulfate solutions may yield to a significant reorganization of the internal microstructure of concrete. In addition to the formation of the new sulfate-bearing products, the penetration of external ions markedly accentuates the dissolution of calcium hydroxide and the decalcification of C–S–H.

The detrimental effects of weak sodium sulfate solutions do not appear to be linked to capillary suction effects.

Numerical simulations confirm that the quality of the concrete put in place is, by far, the main parameter that controls the deterioration process.

References

[1] St-John DA, Poole AW, Sims I. In: Concrete petrography – a handbook of investigative techniques. London, UK: Arnold; 1998. p. 474.
[2] Taylor HFW. Cement Chemistry. second ed. London, UK: Thomas Telford; 1997.
[3] Diamond S, Lee RJ. Microstructural alterations associated with sulfate attack in permeable concretes. In: Marchand J, Skalny J, editors. Materials science of concrete special volume: sulfate attack mechanisms. Westerville, OH, USA: The American Ceramic Society; 1999. p. 123–73.
[4] Brown PW, Doerr A. Chemical changes in concrete due to the ingress of aggressive species. Cem Concr Res 2000;30:411–8.
[5] Brown PW, Badger S. The distributions of bound sulfates and chlorides in concrete subjected to mixed NaCl, $MgSO_4$, Na_2SO_4 attack. Cem Concr Res 2000;30:1535–42.
[6] J. Skalny, J. Marchand, I. Odler, Sulfate attack on concrete. London, UK: E&FN SPON, 2001.
[7] Novak GA, Colville AA. Effloresence mineral assemblages associated with cracked and degraded residential concrete foundation in Southern California. Cem Concr Res 1989;19:1–6.
[8] Haynes H, O'Neill R, Mehta PK. Concrete deterioration from physical attack by salt. Concr Int 1996;18:63–8.
[9] Thorvaldson T, Vigfusson VA, Larmour RK. The action of sulphates on the components of portland cement. Trans Roy Soc Can 1927;21(Sec. III):295–309.
[10] Terzaghi RD. Concrete deterioration in a shipway. J Am Concr Inst 1948;44:977–1005.
[11] Brown PW. An evaluation of the sulfate resistance of cements in a controlled environment. Cem Concr Res 1981;11:719–27.
[12] Schneider U, Piasta WG. The behaviour of concrete under Na_2SO_4 solution attack and sustained compression or bending. Mag Concr Res 1991;43:281–9.
[13] American Concrete Institute, Guide to durable concrete, ACI 201.2R-99. Farmington Hills, Michigan, USA, 1999.
[14] American Concrete Institute, Building code requirements for structural concrete, ACI 318-99. Farmington Hills, Michigan, USA, 1999.
[15] Uniform Building Code, Structural engineering design provisions, vol. 3. Concrete, International Conference of Building Officials; 1977 (Chapter 19).
[16] Canadian Standard Association, A23.1-94, Concrete: constituents and construction practices. Rexdale, Ontario, Canada, 1994.
[17] American Concrete Institute, Slabs on grade, concrete craftsman series. Farmington Hills, Michigan, USA, 1995.
[18] Hamilton JJ, Handegord GO. The performance of ordinary Portland cement concrete in prairies soils of high sulphate content. In: Swenson EG, editor. Performance of concrete-resistance of concrete to sulphate and other environmental conditions: a symposium in honour of Thobergur Thorvaldson. University of Toronto Press; 1968. p. 135–58.
[19] Harboe EM. Longtime studies and field experiences with sulfate attack. In: Sulfate Resistance of Concrete (George Verbeck Symposium), ACI SP-77, 1982. p. 1–20.
[20] DePuy GW. Chemical resistance of concrete, in significance of tests and properties of concrete and concrete-making materials. In: Klieger P, Lamond J, editors. STP 169C. Philadelphia: ASTM; 1994. p. 263–81.
[21] Marchand J. Modeling the behavior of unsaturated cement systems exposed to aggressive chemical environments. Mater Struct 2001;34:195–200.
[22] Marchand J, Bentz DP, Samson E, Maltais Y. Influence of calcium hydroxide dissolution on the transport properties of hydrated cement systems. In: Skalny J, Gebauer J, Odler I, editors. Materials science of concrete special volume: calcium hydroxide in concrete, 2001, pp. 113–129.
[23] Marchand J, Maltais Y, Samson E. Behavior of hydrated cement systems exposed to sodium sulfate solutions, in preparation.
[24] Bear J, Bachmat Y. Introduction to modeling of transport phenomena in porous media. Amsterdam, The Netherlands: Kluwer Academic Publishers; 1991.
[25] Samson E, Marchand J, Beaudoin JJ. Describing ion diffusion mechanisms in cement-based materials using the homogenization technique. Cem Concr Res 1999;29:1341–5.
[26] Marchand J, Samson E, Beaudoin JJ. Modeling ion transport mechanisms in unsaturated porous media. In: Hubbard A, editor. Encyclopedia of surface and colloid science. New York, USA: M. Dekker, 2001, in press.
[27] Helfferich F. Ion exchange. USA: McGraw-Hill; 1961.
[28] Pankow JF. Aquatic chemistry concepts. New York, USA: Lewis Publishers; 1994.
[29] Samson E, Lemaire G, Marchand J, Beaudoin JJ. Modeling chemical activity effects in strong ionic solutions. Comput Mater Sci 1999;15:285–94.
[30] Samson E, Marchand J, Robert J-L, Bournazel J-P. Modelling ion diffusion mechanisms in porous media. Int J Numer Meth Eng 1999;46:2043–60.
[31] Samson E, Marchand J. Numerical solution of the extended Nernst–Planck model. J Colloid Interface Sci 1999;215:1–8.
[32] Pel L. Moisture transport in porous building materials. PhD Thesis, Eindhoven University of Technology, The Netherlands, 1995. p. 125.

[33] Reardon EJ. Problems and approaches to the prediction of the chemical composition in cement/water systems. Waste Manage 1992;12:221–39.
[34] Berner UR. Modelling the incongruent dissolution of hydrated cement minerals. Radiochim Acta 1988;44/45:387–93.
[35] Adenot F, Richet C. Modelling the chemical degradation of a cement paste. In: Scrivener K, Young JF, editors. Mechanisms chemical degradation of cement-based systems. London, UK: E&FN Spon; 1997. p. 341–9.
[36] Faucon P. Concrete durability: physico-chemistry of the alteration by water. PhD Thesis, Cergy-Pontoise University, France, 1997. p. 260 (in French).
[37] Garboczi EJ, Bentz DP. Computer simulation of the diffusivity of cement-based materials. J Mater Sci 1992;27:2083–92.
[38] Powers TC, Brownyard TL. Studies of the physical properties of hardened Portland cement paste (nine parts). J Am Concr Inst 1946–1947;43.
[39] Samson E. Modeling ion transport mechanisms in unsaturated cement systems. PhD Thesis, Department of Civil Engineering, Laval University, Canada, 2001, in preparation.
[40] Longuet P, Burglen L, Zelwer A. In: The liquid phase of hydrated cement, vol. 219. Technical Publication CERILH; 1980. (in French).
[41] Diamond S. Effects of two danish fly ashes on alkali contents of pore solutions of cement fly ash pastes. Cem Concr Res 1981;11:383–90.
[42] Hazrati K. (1995), Investigation of the mechanisms of moisture transport by capillary suction in ordinary and high-performance cement-based materials. PhD thesis, Laval University, Canada, p. 205.
[43] Wang JG. Sulfate attack on hardened cement paste. Cem Concr Res 1994;24:735–42.
[44] Mehta PK. Sulfate attack on concrete: separating the myth from reality. Concr Int 2000;22:57–61.
[45] Tremper B. The effects of acid waters on concrete. J Am Concr Inst 1931;28(9):1–32.
[46] Marchand J, Beaudoin JJ, Pigeon M. Influence of calcium hydroxide dissolution on the engineering properties of cement-based materials. In: Marchand J, Skalny J, editors. Materials science of concrete special volume: sulfate attack mechanisms. Westerville, OH: The American Ceramic Society; 1999. p. 283–94.
[47] Saito H, Deguchi A. Leaching tests on different mortars using accelerated electrochemical method. Cem Concr Res 2000;30:1815–25.
[48] Maltais Y. Ion and fluid transport in hydrated cement systems. PhD Thesis, Department of Civil Engineering, Laval University, Canada, 2001, in preparation.